Erosion and redeposition pattern on the W7-X graphite test divertor unit tile

Elzbieta Fortuna-Zalesna [a,*], Witold Zielinski [a], Łukasz Ciupiński [a], Maciej Spychalski [a], Chandra Prakash Dhard [b], Dirk Naujoks [b], Marcin Rasinski [c], Sebastijan Brezinsek [c], W7-X Team [1]

[a] Faculty of Materials Science and Engineering, Warsaw University of Technology, Woloska 141, Warsaw 02-507, Poland
[b] Max-Planck-Institut für Plasmaphysik, Greifswald D-17491, Germany
[c] Forschungszentrum Jülich, Institut für Energie- und Klimaforschung-Plasmaphysik, Partner of the Trilateral Euregio Cluster (TEC), Jülich 52425, Germany

ARTICLE INFO

Keywords:
Wendelstein 7-X
Plasma-facing components
Plasma-wall interaction
Erosion and deposition
Graphite

ABSTRACT

A set of plasma-facing components was retrieved from the W7-X vessel after OP1.2b campaign with an inertially cooled Test Divertor Unit (TDU) and analyzed postmortem to provide data on the plasma-surface interactions processes in the complex device geometry. In the present study, the lower TDU horizontal target (HT) graphite tile HM19TM400hTE2 exposed to the plasma during both OP 1.2 campaigns was examined. The surface modification of the material caused by the plasma-wall interactions was determined. The study employed several microscopy methods including SEM, FIB, STEM, TEM, EDX, and optical profilometry which showed that (i) distinct erosion zone was located at the inner HT strike line position, (ii) the area covered by a pronounced deposit was located adjacent the erosion zone, (iii) the target finger substructures positioned close to the outboard side was unaltered, and (iv) significant changes to surface roughness values along the length of the plate occurred.

1. Introduction

In future steady-state operated fusion power plants, plasma-wall interactions (PWI) are expected to play a considerable role. In contrast to tokamaks, in stellarators with three-dimensional (3D) plasma geometry and bend shapes such studies are more challenging to describe, limited, and still ongoing (LHD [1–4]). Wendelstein 7-X (W7-X) provides a unique possibility to study PWI phenomena in its specific 3D twisted plasma configuration and island divertor. The obtainment of a greater understanding of PWI underlying physics, the development of the mitigation of erosion, and impurity sources may be possible.

W7-X is an advanced stellarator with a plasma volume of 30 m^3, a major radius of 5.5 m, and superconducting coils, which has been in operation since 2015. After the second operational phase OP1.2 split into two parts OP1.2a and OP1.2b, between 2017−2018 it completed its operation with ten inertially cooled island Test Divertor Units (TDUs) made of graphite, installed in 5 upper (U) and 5 lower (L) parts of the ten half modules (HM). Each TDU consisted of 9 horizontal (h) and 3 vertical (v) target modules (TMs). TM consisted of a certain number of target elements (TEs) i.e., individual tiles. The successful application of this concept has already demonstrated the ancestor experiment W7-AS [5,6].

A set of plasma-facing components was retrieved from W7-X vessel after OP1.2b campaign and analyzed post mortem to provide data on the plasma-surface interactions processes in the complex device geometry [7–9].

The erosion and deposition pattern of carbon at the divertor was studied by investigating a set of 18 special target elements with C/Mo marker layers installed in all 10 divertor HMs and exchanged from the vessel during venting between the campaigns, employing surface analytical methods such as ion beam analysis (IBA), laser-induced spectroscopy, and others [10–14]. The obtained results were used to predict erosion, transport, and deposition in the next campaigns utilizing the actively cooled carbon fiber composite (CFC) divertor intended to enable long pulse operation up to 1800s with the same geometrical design as TDU, which was installed in the machine between 2019−2021. The summary of the plasma-wall interaction studies in W7-X was reported in Ref. [7,8,11]. The main conclusions drawn from the research were summarized as follows:

* Corresponding author.
E-mail address: Elzbieta.Fortuna@pw.edu.pl (E. Fortuna-Zalesna).
[1] W7-X Team are co-authors of the paper, Thomas Sunn Pedersen et al. (2022) *Nucl. Fusion* 62 042022, https://doi.org/10.1088/1741–4326/ac2cf5.

- The plasma operation with the graphite TDU provided vital information regarding PSI processes in W7-X operating with an island divertor.
- Carbon erosion followed the heat and particle footprint on the divertor target plates resulting in strong net erosion zones at the strike lines. The carbon erosion rate at the horizontal tiles normalized to the exposure time in standard divertor configuration was 2.8 ± 0.5 mg/s [7,11].
- Boronizations by oxygen gettering reduced dramatically the carbon erosion and promoted reduced impurity content in the plasma, and access to the stellarator- favorite high density operation in the core [15–17]. During OP1.2b, with a total plasma duration of 9054 s, three boronization processes were carried out with an interval of roughly 3000 s. This experiment showed that boronization should last for 1800s long discharge. However, different techniques, i.e., boron dropper [18] and shift of strike lines using control coils, will be attempted during OP2.1 to extend the operation interval between two boronizations.
- Interpretative ERO2.0 and WallDyn-3D modeling of a typical W7-X plasma reproduced the observed net carbon erosion/deposition pattern and revealed carbon migration paths in the standard divertor configuration [7]. In all cases, the modeling required full 3D treatment in contrast to tokamaks where axial symmetry was assumed.
- The optimized first wall conditions are a prerequisite for the foreseen long-pulse operation in W7-X with the new actively cooled divertor.

The integrated net carbon erosion at the inertially cooled divertor plates corresponds to 2.5 long-pulse discharges of 1800s. The predicted erosion amount of carbon in the divertor would be 7.6 g per discharge, assumed similar conditions to OP1.2B campaign and a maximum erosion of 2–4.5 μm per long pulse at the strike line. Dust production from the unstable layers in deposition zones could impede plasma operation in the second operational period. The release of carbon clusters and dust particles from the disintegrated layers was observed in the machines equipped with actively cooled graphite-based plasma facing components Tore Supra [19] and LHD [20]. Therefore, reduction of erosion via either detached divertor conditions and/or a divertor material with lower erosion yield such as tungsten may be additionally required.

In the presented study, postmortem analyses were performed for the graphite horizontal target element without a marker layer from target module TM4h, which was retrieved from the vessel after the entire OP1.2 campaign. This choice was because in the horizontal part of TDU, marker layers were available only in TM1h to TM3h. The work aimed to examine and confirm that the erosion and redeposition pattern on the tile of the fourth horizontal module was similar to that observed on the marker tiles placed in the first, second, and third horizonal modules.

The obtained erosion-deposition profile was compared to the distributions found on the special target elements.

2. Experimental

In the presented study, the fine graphite horizontal target tile designated as HM19TM400hTE2 from the lower TDU module 1, which was subjected to plasma exposures during both OP 1.2 campaigns was examined. The schematic position of the tile in TDU module is shown in Fig. 1, and image of the HM19TM400hTE2 tile cut into 23 pieces (named P0, P1…P22, samples P6, P9, and P19 were further cut into two pieces and named P6T1, P6T2, P9T1, P9T2, P19T1, and P19T2, respectively) is presented in Fig. 2.

Samples were cut with a blade. First, the target element was cut along the length into two parts, i.e. plasma-facing part and back-side part, to reach the plasma-facing part's thickness of 10 mm. Then the plasma-facing part was cut into the pieces shown in Fig. 2 along the existing groves in the tile. The size of samples P2–P22 was 25 mm x 55 mm. During the cutting process, dedicated vacuum cleaning was employed to minimize contamination of the plasma-facing surface with cutting debris. No additional cleaning was performed.

During OP1.2a in 2017, the total plasma time was 3776 s, 72.2% of the plasma time involved He fueled discharges, and the dominant magnetic configuration was the Standard one [21] (in which the currents in all non-planar coils were the same and the planar coils were switched off). OP1.2b occurred in 2018 and had a total plasma time of 9054 s in H plasma. Most discharges were in Standard configuration (4809 s). It should be noted that the standard configuration had the strike line on the horizontal target modules TM1h to TM4h and the vertical target modules TM1v to TM3v.

During the operational phase OP1.2a, wall conditioning was performed using glow discharge cleaning without the boronization process. This resulted in very high erosion of carbon at TDU strike line position due to the high levels of oxygen (level of 6%–7% [22]). In the subsequent operational phase OP1.2b, three boronization processes were applied (glow discharges in a 10%B_2H_6 + 90%He mixture), resulting in a decrease of low Z impurity concentration and 5.4-fold reduction of the net erosion rate on the horizontal targets [7,10,22]. The details concerning the plasma operation during OP1.2 were reported in Ref. [7,10,11,22,23].

The surface morphology and composition of the tile as well as the internal features of the deposit were examined with several microscopy methods, including scanning electron microscopy (Hitachi SU-8000 FE-SEM) combined with energy-dispersive X-ray spectroscopy (EDX - Thermo Scientific Ultra Dry), focused ion beam (FIB/SEM, Hitachi FB-

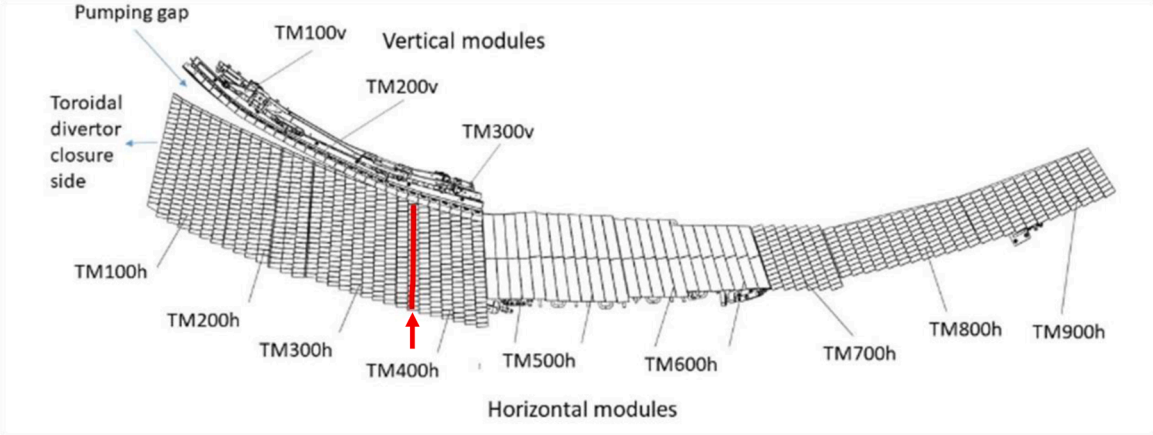

Fig. 1. Drawing of TDU modules (horizontal 9 modules + vertical 3 modules) based on the Max-Planck-Institut für Plasmaphysik's internal document 1-ACT00AC-Z0001. Examined tile position of TDU modules is marked by a thick red line and indicated with a thick red arrow in target module TM400h.

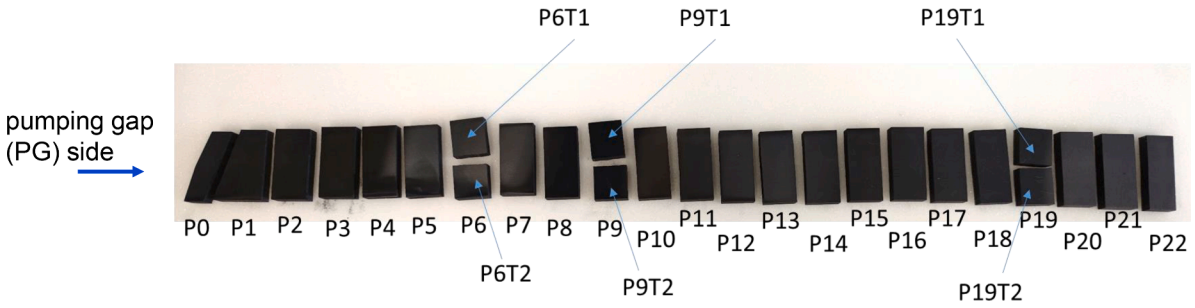

Fig. 2. Image of tile HM19TM400hTE2 cut into 23 samples named P0, P1 …P22. Three samples P6, P9, and P19 were further cut into two pieces each and named P6T1, P6T2, P9T1, P9T2, P19T1, and P19T2, respectively.

2100), scanning transmission electron microscopy (STEM, Hitachi 5500) combined with energy-dispersive X-ray spectroscopy (EDX Thermo Scientific) and transmission electron microscopy (TEM, JOEL 1200 EX). Surface development was determined by optical profilometer Wyko NT9300. Measurements were carried out on each sample in the central part at two magnifications 2.9 and 11.5 times. The roughness average value Ra was calculated from the areas with dimensions equal to 1.7×2.2 mm^2 and 412×550 μm^2, respectively. The average number of measurements of each sample was 4 and 8 for a magnification of 2.9 and 11.5x, respectively.

3. Results

3.1. Surface morphology

SEM examinations revealed that the surface of the majority of examined samples was modified after exposure to OP1.2 campaign conditions as evidenced by the images shown in Figs. 3–6.

The erosion zone was observed on samples P5, P6T1, and P7. Micrographs that displayed surface features of this area in conjunction with EDX spectra are shown in Fig. 3. The surface of the material in this region was smoothened with traces of impurities in the shallow cavities at the surface (shadowed areas). This effect was also observed in the eroded areas of the graphite limiters from the TEXTOR tokamak [24]. EDX spectra showed only a carbon peak at the eroded zones (Fig. 3e), whereas peaks related to oxygen and small ones from other elements (like Fe, Cl, S) were observed inside the shallow cavities (visible in bright contrast in the backscattered electrons (BSE) image) (Fig. 3d). This peak erosion zone was located at approx. $s = 150$ mm, at the location of the inner strike line in standard divertor configuration (with s coordinate origin at the pumping gap of the horizontal target on sample P0 in the middle).

The deposition zone was located adjacent to the erosion zone. As shown in Fig. 4a–b, the surface of samples P8 and P9T1 were covered with a distinct, thick, scale-like deposit. In the case of sample P10, a relatively flat and thinner scale was observed. The registered EDX spectra proved that the main deposit constituents were carbon and oxygen. Additionally, the deposit included a small amount of iron and other steel components along with other impurities (S, Cl, and Na). It should be noted that S and Cl were not determined as exogenous impurities but were found in the deposits of the limiters after OP1.1 campaign [25].

It was found that the target finger substructures located close to the outboard side did not show any evidence of redeposition or erosion (samples P17-P22). As shown in Fig. 5a–b, sample P21 possessed a tile surface in this zone, which was strongly developed, porous, and without characteristic directionality. The obtained EDX spectra showed only the presence of C signal (Fig. 5c). Hence, it was assumed that the morphology of the material in this area was similar to the original plate surface.

In addition to the above-described regions, two transition zones were localized: (i) on the left from the erosion zone, towards the pumping gap

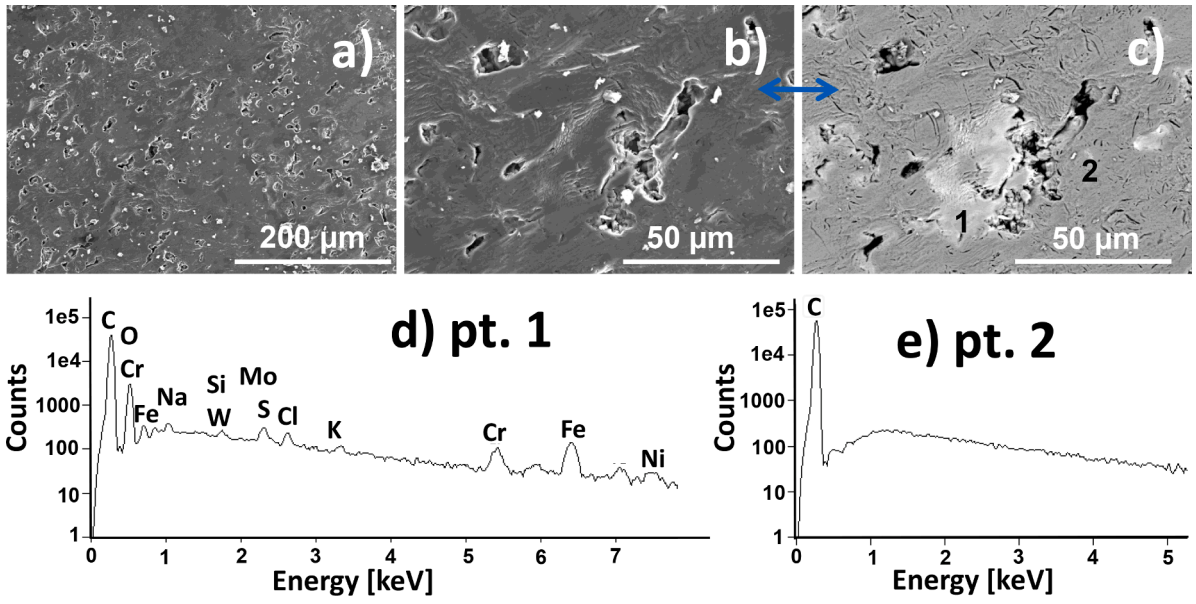

Fig. 3. SEM images of sample P6T1 morphology (a-c) with corresponding EDX spectra (d-e) at points 1 and 2 marked in (c), from the erosion zone. Point 1 is located in the shallow cavity, while point 2 is at the flat surface. Images 3c and 3d show the same location imaged in SE and BSE modes, respectively.

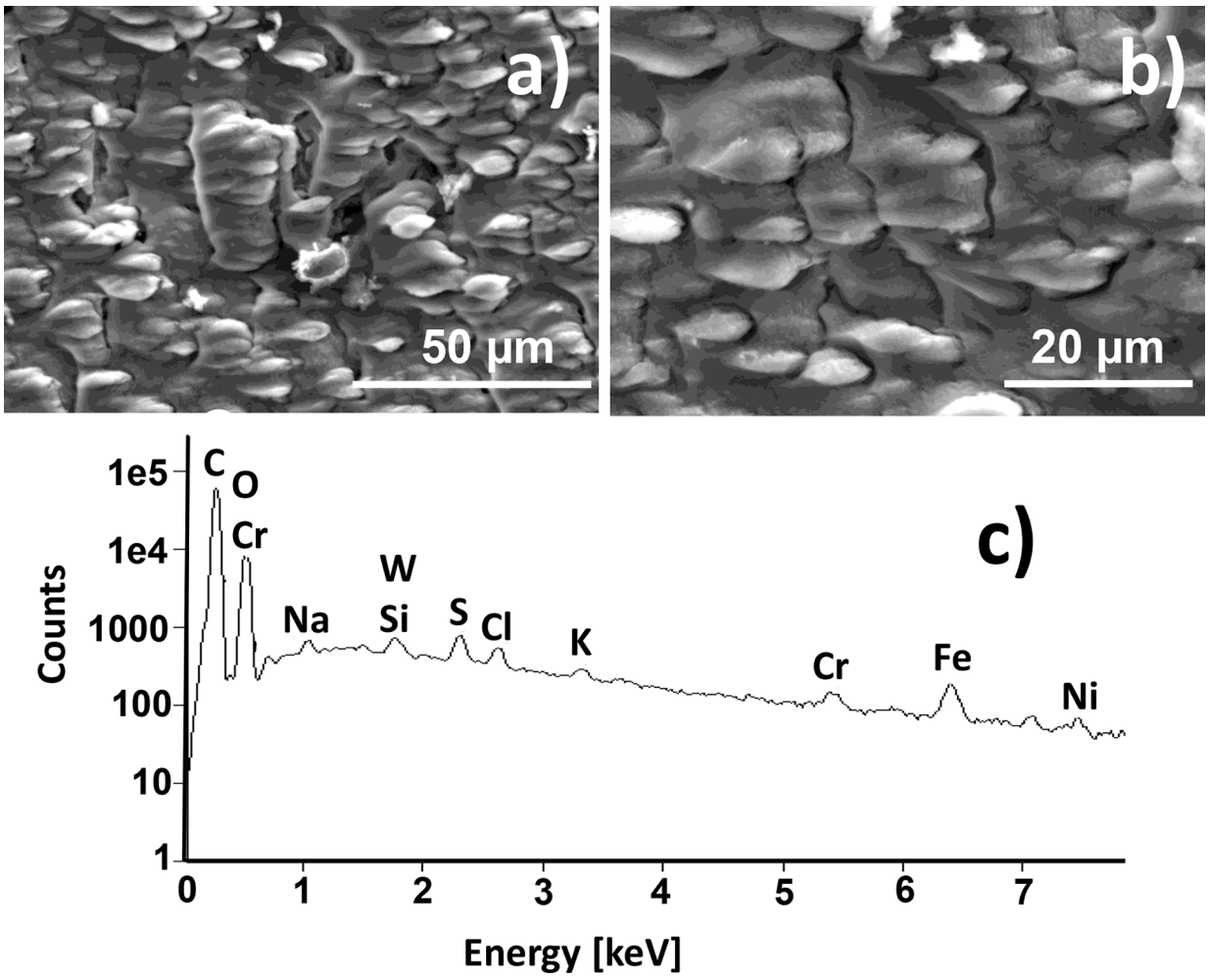

Fig. 4. SEM images of sample P9T1 morphology (a-b) with corresponding EDX spectrum of area (c), in the deposition zone.

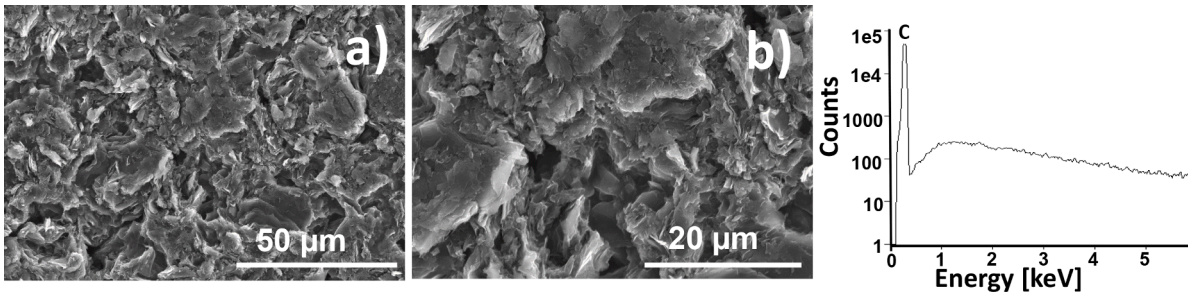

Fig. 5. SEM images of sample P21 morphology (a-b) with corresponding EDX spectrum of area (c), located in the region without direct plasma contact.

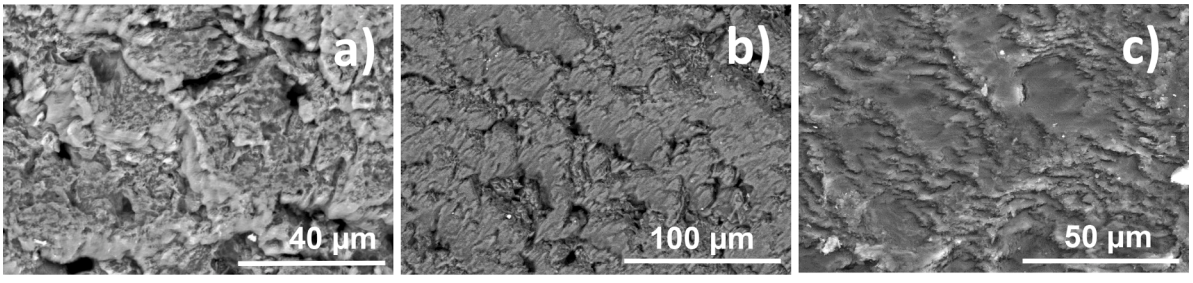

Fig. 6. SEM images of the surface morphology in the first transition zone: (a) sample P0, (b) sample P1, (c) sample P3.

side, and (ii) on the right from the region with strong redeposition. The first transition zone comprised of samples P0–P4. It should be noted that the surface morphology in this region was diversified (Fig. 6). In the case of sample P0, neither a clear layer of deposit nor a strongly eroded surface was detected. However, at the edges of the pores/surface cavities, a concentration of impurities was observed. Sample P1 was covered by a deposit. Sample P2 was partially eroded, although EDX measurements confirmed the presence of impurities on the surface indicating redeposition. Sample P3 showed another type of morphology, where the surface appeared to be trimmed with a razor. Part of sample P4 surface was significantly eroded, whereas another part had similar morphology to sample P3. In all cases, the characteristic surface directionality (the same direction as for the eroded areas) was determined.

The character of the surface in the second transition zone (samples P12-P16) was different, in which a gradual shift occurred from the redeposition to the unaltered zone.

3.2. TEM investigations

3.2.1. Deposit internal structure

TEM images showing the structure of deposit grown on the surface of sample P9T1 and the corresponding electron diffraction pattern are presented in Fig. 7. The structure of the deposit was inhomogeneous and contained areas with significantly different porosity. Additionally, the layered structure of the deposit material was obvious. The deposit layer thickness was determined by TEM images and reached 2.7 μm. The electron diffraction pattern shown in Fig. 7c, displays weak, diffused rings that indicated the material's amorphous structure.

TEM analysis was complemented by EDX elemental mapping shown in Fig. 8, which displays the distribution of the main deposit constituents, carbon and oxygen, and revealed the enrichment of the deposit layer with oxygen. A comparable increase was reported previously [12]. The obtained result was consistent with the measurements carried out in the micro-areas on the surface.

The bright and dark field STEM images recorded at 30 kV shown in Fig. 9 revealed that a certain amount of small particles were located in the porous layers of the deposit, but their precise identification was difficult. However, we supposed that these particles may be Fe-enriched regions. The iron enrichment was revealed in the iron profile of the redeposition zone at the divertor target (Fig. 14 in Sereda et al. [15]). The observed increase was related to He glow-discharge cleaning being performed frequently before boronization.

3.2.2. Sub-surface structure in the region without direct plasma contact

To examine the subsurface structure of the samples from the unchanged zone located close to the outboard side, a thin foil was cut out for TEM observation of sample P19T1. Images shown in Fig. 10 display both the sub-surface and graphite matrix structure. No deposit on the surface of the material was observed.

3.3. Roughness measurements

The image shown in Fig. 11 described changes in the surface roughness along the length of the tile at two magnifications 2.9 × and 11.5 × . For the executed series of measurements, the values of standard deviation were relatively small and therefore were excluded from the graph. These amounted to 0.06 and 0.13 μm on average for magnifications of 2.9 × and 11.5 ×, respectively.

The obtained results showed very good agreement for the roughness distribution for both magnifications. The study revealed significant differences in surface roughness values along the length of the tile. Ra parameter for the strongly eroded zone reached the lowest level of 1.6–1.9 μm (mag. 11.5 ×). The value showed a slight increase for the area with a deposit (2.3–2.5 μm), whereas the areas that did not show significant surface damage were characterized by relatively high surface roughness, exceeding 3 μm.

4. Discussion

This section is divided into two parts. The first part briefly describes the erosion-deposition patterns obtained for TM2h6 horizontal target elements used in all TDUs for the study of toroidal erosion asymmetry. In the second part, the erosion-deposition profile is described and compared to the distributions previously detected on the special target elements.

4.1. Erosion-deposition patterns on the special target elements

In the case of PWI investigations, 18 exchangeable divertor target elements with C/Mo marker layers were exposed during the operational phase OP1.2a and OP1.2b. The entire set of target elements was exchanged between the operational phases OP1.2a and OP1.2b. Position TM2h6 (target element/individual tile located in the second horizontal target module, sixth in a row) in the horizontal target was used in all TDUs to study the toroidal asymmetry of the erosion/deposition pattern. Additionally, positions TM1h3 and TM3h6 in the horizontal modules and TM1v5 and TM2v2 in the vertical modules were used in TDUs 5 L and 5 U.

The comprehensive studies of the marker layer thickness changes were determined by elastic backscattering spectrometry (EBS) after the first experimental campaign OP1.2a [10] and revealed a substantial degree of erosion of up to 20 μm of carbon at the strike line. The eroded area ranged from 0 mm to approx. 320 mm and was relatively wide. The thicknesses of the carbon layer remained unchanged in areas without direct plasma contact located close to the outer baffle (320 nm to 470 mm). In remote areas close to the outboard side, a thin deposit was confirmed.

The erosion/deposition patterns observed on all ten TDUs on target element TM2h6 after OP1.2b were similar, however, due to regular boronizations in OP1.2b, the erosions were considerably reduced compared to OP1.2a [11]. High carbon erosion occurred at the strike

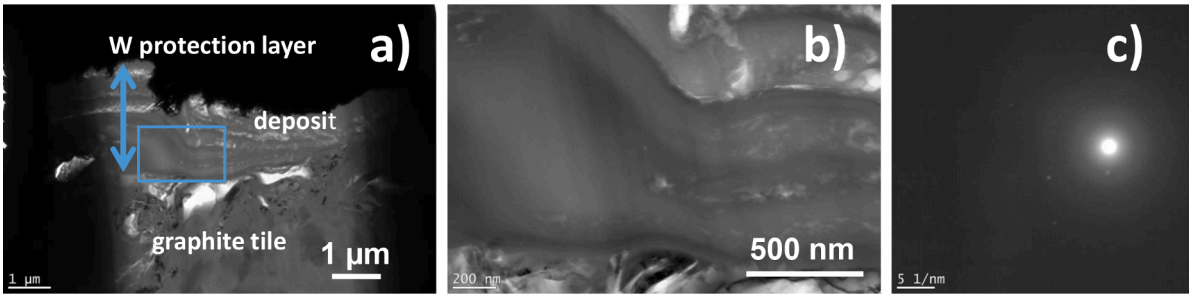

Fig. 7. TEM images of the deposit structure (a-b) with the corresponding electron diffraction pattern (c), sample P9T1. Fig. b shows an enlarged image of the deposit marked with a frame in Fig. a.

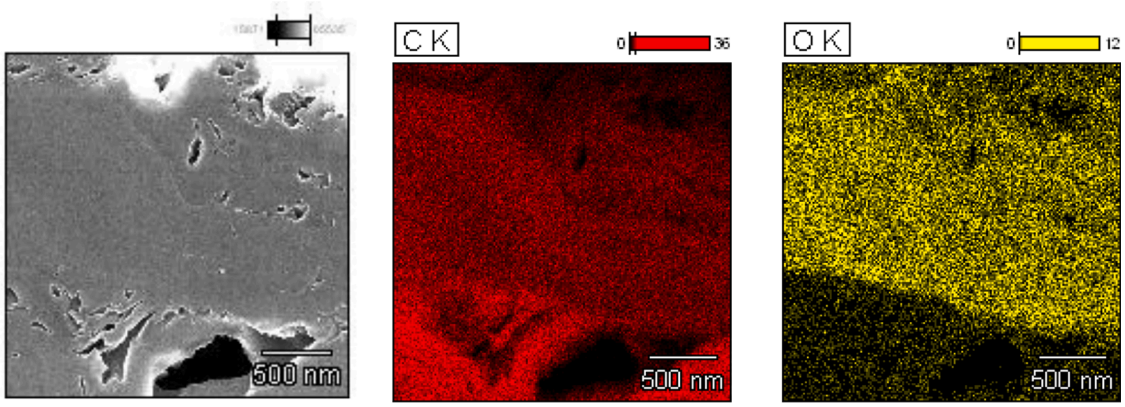

Fig. 8. Distribution of carbon and oxygen in the deposit area, thin foil, sample P9T1.

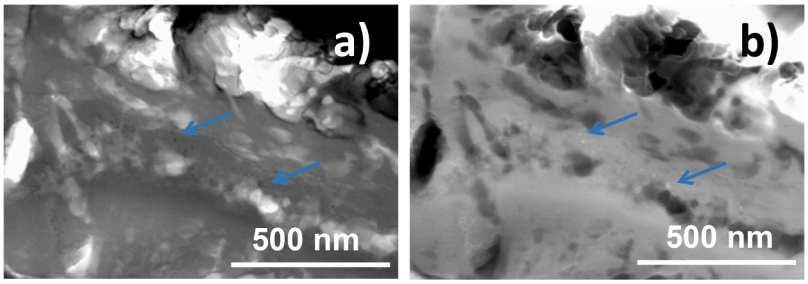

Fig. 9. STEM images of the deposit structure on sample P9T1, recorded in (a) bright and (b) dark field. The arrows indicate the deposited particles.

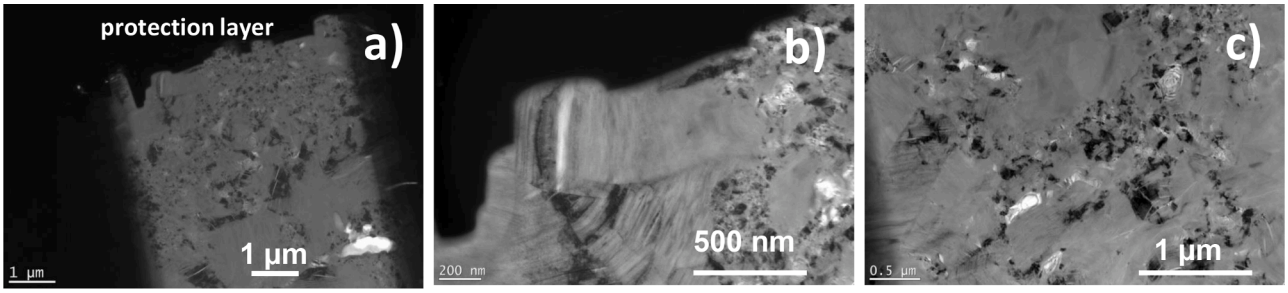

Fig. 10. TEM images of the structure of the material cut out from sample P19T1 from the region without direct plasma contact.

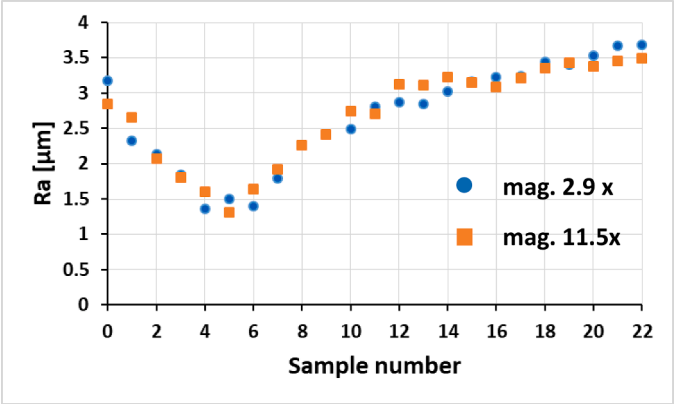

Fig. 11. Changes in surface roughness, Ra along the length of the tile. Measurements carried out at the magnifications of 2.9 and 11.5 show good agreement.

line, in the range of s coordinates ~ 80–200 mm. On the left-hand side of the erosion zone, at position approx. 70 mm, a small deposition of carbon was detected in some TDUs. To the right of the erosion zone, at approx. 250 mm, deposition was detected on all TDUs. Additionally, a second, weaker erosion zone was revealed at s coordinates 320–370 mm, which corresponded to the strike line of Low Iota configuration. The areas towards the baffles showed almost no changes. In contrast to TM2h6 target elements, 5 L TM1h3 tile displayed no erosion at the strike line position, but target element 5 U TM1h3 showed a very similar erosion pattern to TM2h6 target elements.

For both campaigns, TDUs in module 2 had the highest erosion, while the erosion on TDU 5 L was the lowest. For both periods, the erosion in the area with the strongest erosion was twice as high as in the area with the lowest (probably due to asymmetries in power fluxes, which were determined by thermographic measurements). The erosion pattern varied not only between the different target modules in one TDU but also among the different TDUs.

It should be noted that before the marker layer deposition the graphite tiles were ground to obtain a comparable surface finish to the other graphite tiles installed in W7-X. After exposure, their surface was generally smoother than the initial one [10,11].

The lesson learned from both campaigns was a very small deposition of carbon in the remote areas of the divertor with little plasma contact. This was clearly different from that observed in tokamaks, where eroded material redeposited in the remote divertor areas or the inner divertor [26,27].

4.2. Erosion-deposition profile on the horizontal target HM19TM400hTE2

The presented study provides information on the morphological changes of the graphite horizontal target element without marker layer HM19TM400hTE2, from target module 4 h, which was subjected to plasma exposures during the entire OP1.2 campaign. This choice was due to the availability of the marker layers only in target modules TM1h to TM3h.

The investigations revealed distinct erosion zones located in the region of the inner HT strike line position. The peak erosion was found for sample P5, located at the s coordinate 150 mm. The width of this zone, which comprised of part of sample P4 and samples P5–7, amounted to ~10.5 cm. This range corresponded well to the strike line widths of up to 11 cm observed using infrared tomography [28]. The surface in this region was distinctly smoothed, however, small amounts of impurities were detected in the shallow cavities present at the surface. On the right-hand side of the erosion zone, the area was covered by a distinct deposit, particularly for samples P8 and P9 (~5.5 cm). TEM analysis revealed the redeposited layer with a thickness of up to 2.7 μm. The main deposit components were determined as carbon and oxygen and included a small amount of iron and other steel constituents originating from the stainless steel panels and structures. The target finger substructures located close to the outboard side did not show any evidence of redeposition or erosion (samples P17−22). TEM analysis proved that no deposition occurred in this region. In addition to the above-described regions, two transition zones were localized: (i) on the left side of the erosion zone, towards the pumping gap side and (ii) on the right side from the region with strong redeposition. The first transition zone comprised of samples P0−4. It should be noted that the surface morphology in this region was diversified with deposition on sample P1. The character of the surface in the second transition zone (samples P12−16) was different. A gradual shift was observed from redeposition to the unaltered zone.

Importantly, the erosion-deposition pattern present on the examined tile was the result of the processes occurring in the device during both experimental campaigns, i.e., OP1.2a and OP1.2b. The relatively broad erosion peak visible on the graph presenting changes to the roughness along the tile length, which was comprised of samples P1−11, included also the samples that were covered with a thick deposit layer. Its presence was explained (i) by the presence of a large eroded area after the first campaign and (ii) due to the deposit itself possessing a lower roughness than the plate in its initial state. The only difference to the patterns obtained for tiles with marker layers studied after OP1.2b was the lack of the second, weaker erosion zone since the strike line in the low iota magnetic configuration was not particularly dominant on this target tile (Fig. 4 in Renner et al. [29]). Hence, the qualitative shape of the erosion-deposition pattern observed after OP1.2b on target elements TM2h6 and tile HM19TM400hTE2 was comparable.

5. Concluding remarks

In the present study, postmortem analyses were performed on the graphite horizontal target element without a marker layer from target module TM4h, retrieved from the vessel after the entire OP1.2 campaign. This was examined because in the horizontal part of TDU, marker layers were available only in TM1h to TM3h. The work aimed to investigate whether the erosion and redeposition pattern on the tile of the fourth horizontal module was similar to the one observed on the marker tiles placed in the first, second, and third horizonal modules. It was confirmed that the erosion-deposition pattern observed on the marker tiles and the graphite tile from the fourth horizontal module were comparable.

In addition, the research allowed the determination of changes that occurred on a real W7-X graphite tile (so far, these changes could only be tracked on marker tiles), as well as quantitatively showed surface roughness modifications. Importantly, it has been already shown experimentally and by computer simulations that the physical sputtering yield of a rough surface can deviate significantly from a smooth surface [30–34]. The smoothing effect of the plasma exposure of initially rough surfaces by erosion/deposition processes observed on the marker tiles was confirmed both quantitatively (by roughness measurements) and qualitatively (by microscopic observations of the surface).

Declaration of Competing Interest

The authors declare that they have no known competing financial interests or personal relationships that could have appeared to influence the work reported in this paper.

Data availability

No data was used for the research described in the article.

Acknowledgments

This work has been carried out within the framework of the EUROfusion Consortium, funded by the European Union via the Euratom Research and Training Programme (Grant Agreement No 101052200 — EUROfusion). Views and opinions expressed are however those of the author(s) only and do not necessarily reflect those of the European Union or the European Commission. Neither the European Union nor the European Commission can be held responsible for them. This work was performed under EUROfusion WPPWIE. It was supported by Ministry of Science and Higher Education of Poland from financial appropriations for science in 2022, granted for the implementation of the international co-financed project.

References

[1] V. Alimiov, M. Yajima, S. Masuzaki, M. Tokitani, Analysis of mixed-material layers deposited on the toroidal array probes during the FY 2012 LHD plasma campaign, Fusion Eng. Des. 147 (2019), 111228.
[2] Y. Oya, C. Hu, H. Fujita, J. Uemura, S. Sakurada, et al., Influence of mixed material layer formation on hydrogen isotope and He retentions in W exposed to 2014 LHD experiment campaign, Fusion Eng. Des. 128 (2017) 458.
[3] M. Tokitani, N. Yoshida, M. Miyamoto, T. Hino, Y. Nobuta, et al., Characterization of surface modifications of plasma-facing components in LHD fusion, *Sci.* Tech. 58 (2010) 305.
[4] G. Motojima, N. Yoshida, S. Masuzaki, R. Sakamoto, M. Tokitani, et al., Wide-range evaluation of the deposition layer thickness distribution on the first wall by reflection coefficient measurements, Nucl. Mat. Energy 12 (2019) 1219.
[5] M. Hirch, J. Baldzuhn, C. Beidler, R. Brakel, R. Burhen, et al., Major results from the stellarator wendelstein 7-AS, Plasma Phys. Control. Fusion 50 (2008), 053001.
[6] R. König, P. Grigull, K. McCormick, Y. Feng, H. Ehmler, et al., Divertors for helical devices: concepts, plans, results, and problems, Fusion Sci. Technol. 46 (2004) 152–166.
[7] S. Brezinsek, C.P. Dhard, M. Jakubowski, R. König, S. Masuzaki, et al., Plasma–surface interaction in the stellarator W7-X: conclusions drawn from operation with graphite plasma-facing components, Nucl. Fusion 62 (2022), 016006.
[8] C.P. Dhard, S. Brezinsek, M. Mayer, D. Naujoks, S. Masuzaki, et al., Plasma-wall interaction studies in W7-X: main results from the recent divertor operations, Phys. Scr. 96 (2021), 124059.
[9] C.P. Dhard, S. Äkäslompolo, M. Balden, J. Baldzuhn, C. Biedermann, et al., Inspection of W 7-X plasma-facing components after the operation phase OP1.2b: observations and first assessments, Phys. Scr. T171 (2020), 014033.
[10] M. Mayer, M. Balden, S. Brezinsek, V.V. Burwitz, C.P. Dhard, et al., Material erosion and deposition on the divertor of W7-X, Phys. Scr. T171 (2020), 014035.
[11] M. Mayer, M. Balden, S. Brezinsek, V.V. Burwitz, C. Cupak, et al., Carbon erosion/deposition on the divertor of W7-X during the operational period OP 1.2b, Nuclear Fusion 62 (2022), 126049.

[12] C.P. Dhard, M. Mayer, S. Brezinsek, S. Masuzaki, G. Motojima, et al., Erosion and deposition investigations on Wendelstein 7-X first wall components for the first operation phase in divertor configuration, Fusion Eng. Des. 14 (2019) 242.
[13] D. Zhao, R. Yi, J. Oelmann, S. Brezinsek, M. Rasinski, et al., *Ex situ* analysis of W7-X divertor plasma-facing components by picosecond laser diagnostics, Phys. Scr. T171 (2020), 014018.
[14] D. Zhao, R. Yi, A. Eksaeva, J. Oelmann, S. Brezinsek, et al., Quantification of erosion pattern using picosecond-LIBS on a vertical divertor target element exposed in W7-X, Nucl. Fusion 61 (2021), 016025.
[15] S. Sereda, S. Brezinsek, E. Wang, T. Barbui, R. Brakel, et al., Impact of boronizations on impurity sources and performance in Wendelstein 7-X, Nucl. Fusion 60 (2020), 086007.
[16] E. Wang, S. Brezinsek, S. Sereda, B. Buttenschön, T. Barbui, et al., Impurity sources and fluxes in W7-X: from the plasma-facing components to the edge layer, Phys. Scr. T171 (2020), 014040.
[17] J. Winter, Wall conditioning in fusion devices and its influence on plasma performance, Plasma Phys. Control Fusion 38 (1996) 1503.
[18] R. Lunsford, C. Killer, A. Nagy, D.A. Gates, T. Klinger, et al., Characterization of injection and confinement improvement through impurity induced profile modifications on the Wendelstein 7-X stellarator, Phys Plasmas 28 (2021), 082506.
[19] E. Tsitrone, C. Brosset, B. Pegourie, E. Gauthier, J. Bouvet, et al., Deuterium inventory in Tore Supra: reconciling particle balance and post-mortem analysis, Nucl. Fusion 49 (2009), 075011.
[20] M. Tokitani, H. Kasakara, S. Masuzaki, G. Motojima, M. Shoji, et al., Plasma wall interaction in long-pulse helium discharge in LHD – microscopic modification of the wall surface and its impact on particle balance and impurity generation, J. Nucl. Mater 463 (2015) 91.
[21] J. Geiger, C.D. Beidler, Y. Feng, H. Maaßberg, N.B. Marushchenko, Y. Turkin, Physics in the magnetic configuration space of W7-X, Plasma Phys. Control. Fusion 57 (2015), 014004.
[22] M. Mayer, M. Kandler, C.P. Dhard, S. Elgeti, Y. Gao, et al., Assessment of carbon net erosion/deposition at the divertor of W7-X, Nuclear Mat. Energy 34 (2023), 101352.
[23] M. Mayer, M. Balden, S. Brezinsek, C.P. Dhard, S. Elgeti, et al., Erosion of tungsten marker layers in W7-X, Phys. Scr. 96 (2021), 124070.
[24] M. Rubel, E. Fortuna, A. Kreter, E. Wessel, V. Philipps, K. Kurzydłowski, Overview of comprehensive characterisation of erosion zones on plasma facing components, Fusion Eng. Des. 81 (2006) 211–219.
[25] V.R. Winters, S. Brezinsek, F. Effenberg, M. Rasinski, O. Schmitz, et al., Overview of the plasma-surface interaction on limiter surfaces in the startup campaign of Wendelstein 7-X, Phys. Scr. T170 (2017), 014050.
[26] S. Brezinsek, A. Widdowson, M. Mayer, V. Philipps, P. Baron-Wiechec, et al., Beryllium migration in JET ITER-like wall plasmas, Nucl. Fusion 55 (2015), 063021.
[27] A. Kirchner, S. Brezinsek, A. Huber, A. Meigs, G. Sergienko, et al., Modelling of tungsten erosion and deposition in the divertor of JET-ILW in comparison to experimental finding, Nucl. Mater. Energy 18 (2019) 234–244.
[28] T.S. Pedersen, R. König, M. Krychowiak, M. Jakubowski, J. Baldzuhn, et al., First results from divertor operation in Wendelstein 7-X, Plasma Phys. Control. Fusion 61 (2019) 01403.
[29] H. Renner, J. Boscary, V. Erckmann, H. Greuner, H. Grote, et al., The capabilities of steady state operation at the stellarator W7-X with emphasis on divertor design, Nucl. Fusion 40 (2000) 1083.
[30] M. Küstner, W. Eckstein, V. Dose, J. Roth, The influence of surface roughness on the angular dependence of the sputter yield, Nucl. Instrum. Methods Phys. Res. B 145 (1998) 320.
[31] M. Küstner, W. Eckstein, E. Hechtl, J. Roth, Angular dependence of the sputtering yield of rough beryllium surfaces, J. Nucl. Mater. 265 (1999) 22.
[32] U. von Toussaint, A. Mutzke, A. Manhard, Sputtering of rough surfaces: a 3D simulation study, Phys. Scr. T170 (2017), 014056.
[33] R. Arredondo, M. Oberkofler, T. Schwarz-Selinger, U. von Toussaint, V.V. Burwitz, et al., Angle-dependent sputter yield measurements of keV D ions on W and Fe and comparison with SDTrimSP and SDTrimSP-3D, Nucl. Mater. Energy 18 (2019) 72.
[34] M. Kelemen, T. Schwarz-Selinger, A. Mutzke, M. Balden, E. Vassallo, et al., Influence of surface roughness on the sputter yield of Mo under keV D ion irradiation, 2021, J. Nucl. Mater. 555 (2021), 153135.